## Deep Search for Molecular Oxygen in TW Hya

Becky J. Williams, L. Ilsedore Cleeves, Christian Eistrup, AND Jon P. Ramsey

Department of Astronomy, University of Virginia, Charlottesville, VA 22904, USA
 Max Planck Institute for Astronomy, Königstuhl 17, 69117 Heidelberg, Germany

# ABSTRACT

The dominant form of oxygen in cold molecular clouds is gas-phase carbon monoxide (CO) and ice-phase water (H<sub>2</sub>O). Yet, in planet-forming disks around young stars, gas-phase CO and H<sub>2</sub>O are less abundant relative to their ISM values, and no other major oxygen-carrying molecules have been detected. Some astrochemical models predict that gas-phase molecular oxygen (O<sub>2</sub>) should be a major carrier of volatile oxygen in disks. We report a deep search for emission from the isotopologue <sup>16</sup>O<sup>18</sup>O ( $N_J = 2_1 - 0_1$  line at 233.946 GHz) in the nearby protoplanetary disk around TW Hya. We used imaging techniques and matched filtering to search for weak emission but do not detect <sup>16</sup>O<sup>18</sup>O. Based on our results, we calculate upper limits on the gas-phase O<sub>2</sub> abundance in TW Hya of  $(6.4-70) \times 10^{-7}$  relative to H, which is 2-3 orders of magnitude below solar oxygen abundance. We conclude that gas-phase O<sub>2</sub> is not a major oxygen-carrier in TW Hya. Two other potential oxygen-carrying molecules, SO and SO<sub>2</sub>, were covered in our observations, which we also do not detect. Additionally, we report a serendipitous detection of the C<sup>15</sup>N  $N_J = 2_{5/2} - 1_{3/2}$  hyperfine transitions, F = 3 - 2 and F = 2 - 1, at 219.9 GHz, which we found via matched filtering and confirm through imaging.

Keywords: protoplanetary disks, astrochemistry

#### 1. INTRODUCTION

Protoplanetary disks provide a critical link in understanding the chemical evolution from the interstellar medium (ISM) to planetary systems (including our own solar system). By studying these environments, we can understand how molecular abundances change as stars, and later planets, form. Such observations are helpful to put our own solar system into context. So far, there have been about 300 unique molecules (not including isotopologues) detected in the ISM. Within protoplanetary disks, only 25 unique molecules have been detected (McGuire 2022). This low detection rate is not due to decreased chemistry in disks, but because we do not know some of the key tracers of the most abundant elements, such as oxygen.

Oxygen is the third most abundant element in the Universe, with a solar oxygen abundance of  $4.9 \times 10^{-4}$  relative to hydrogen (Asplund et al. 2009, 2021). The vast majority of oxygen in the Universe is incorporated into gas-phase molecules, ice-phase molecules, or refrac-

Corresponding author: Becky J. Williams rjw9dmj@virginia.edu

tory dust. Whittet (2010) considered the incorporation of oxygen into silicates and oxides and estimated that the amount of oxygen in dust is  $(0.9-1.4)\times10^{-4}$  relative to hydrogen in different ISM environments.

van Dishoeck et al. (2021) discuss the oxygen budget of ISM environments, assuming a total oxygen abundance of  $5.8 \times 10^{-4}$  relative to hydrogen (Przybilla et al. 2008). They note that about 20% of the total abundance of oxygen is unaccounted for in diffuse clouds, increasing to 50% in dense regions. Two of the most common molecules in the ISM and protoplanetary disks are carbon monoxide (CO) and water (H<sub>2</sub>O). In warm gas in the interstellar medium, gas-phase CO has an abundance of about  $10^{-4}$  relative to hydrogen (Ripple et al. 2013), but is observed to be less abundant in protoplanetary disks (Dutrey et al. 1994; Ansdell et al. 2016; Long et al. 2017). Similarly, water ice has an abundance of  $H_2O/H_2 \approx 10^{-4}$  in dense clouds (see van Dishoeck et al. 2013), but water vapor has been detected in low abundance in only a few disks (Du et al. 2017). It is possible that a large amount of oxygen is in frozen species, such as water ice, that are difficult to observe. Another possibility is that oxygen is in other gas-phase molecules, such as molecular oxygen  $(O_2)$ .

 $O_2$  has been observed in low abundances in two molecular clouds:  $O_2/H_2\approx (0.3-7.3)\times 10^{-6}$  in Orion (Goldsmith et al. 2011) and  $O_2/H_2\approx 5\times 10^{-8}$  in  $\rho$  Oph A (Liseau et al. 2012).  $O_2$  is a reactive molecule, and its most common form,  $^{16}O^{16}O$ , is difficult to detect due to a lack of a permanent dipole moment. The less-abundant isotopologue  $^{16}O^{18}O$  does, however, have a dipole moment. Through this isotopologue,  $O_2$  was tentatively detected in the protostellar system IRAS 16293-2422 B (Taquet et al. 2018). There have been no other reported detections of  $O_2$  in protoplanetary disks.

Interestingly,  $O_2$  has been detected in our own solar system in comets, which we do not expect to have undergone much chemical evolution since their formation in the pre-solar nebula. For example,  $O_2$  was detected in the coma of comet 67P/Churyumov-Gerasimenko (67P) by the ROSINA (Balsiger et al. 2007) instrument on ESA's Rosetta spacecraft. Bieler et al. (2015) found an unexpectedly high average O2 to water ratio of  $3.80 \pm 0.85\%$ , making  $O_2$  the fourth most abundant species in the coma.  $O_2$  was also detected in comet 1P/Halley at an abundance of  $3.7 \pm 1.7\%$  relative to water (Rubin et al. 2015). In both cases,  $O_2$  and  $H_2O$ abundance appear to be correlated. As described in Luspay-Kuti et al. (2018, and references therein), there have been many proposed origins for O<sub>2</sub> in comets, ranging from in situ processes to origins in the ISM prior to formation of the solar nebula. Recent analysis by Luspay-Kuti et al. (2022) shows that, farther from the Sun, O<sub>2</sub> abundance in 67P is more strongly correlated with CO and  $CO_2$  than with  $H_2O$ . They suggest that 67P has two reservoirs of O<sub>2</sub>: a deep primordial nucleus of CO and CO<sub>2</sub> ice, and a surface layer of H<sub>2</sub>O ice that formed later.

If  $O_2$  in comets is not formed in situ, then it must have been present in the protoplanetary disk from whence the comet formed. This scenario is supported by chemical models that predict a large amount of oxygen is in gasphase  $O_2$  in the inner regions of disks. For example,  $O_2$  ice can be produced on dust grain surfaces and under certain conditions desorbs faster than it reacts to form other molecules. Eistrup et al. (2018) predict that this process occurs in the midplane of disks, resulting in a build-up of gas-phase O<sub>2</sub> between the H<sub>2</sub>O and O<sub>2</sub> ice lines (between 0.7 and 10 au after 8 million years). Walsh et al. (2015) meanwhile predict that gas-phase O<sub>2</sub> builds up in the atmosphere of T Tauri disks, produced via gas-phase neutral-neutral reactions of O + OH. They predict that  $O_2$  may carry 50% of the total oxygen in the disk's atmosphere, and 10% when including the midplane.

In this paper, we present a deep search for  $^{16}\mathrm{O}^{18}\mathrm{O}$  emission in ALMA observations of TW Hya, a well-studied T Tauri protoplanetary disk. TW Hya's relatively gas-rich disk and nearby proximity make it a good candidate for searching for faint emission. There have been many observations of gas emission lines in TW Hya, and previous observations have shown that CO gas is 1-2 orders of magnitude less abundant than in the ISM (Favre et al. 2013; Cleeves et al. 2015). Water vapor has a maximum observed abundance of  $\mathrm{H_2O/H_2} \approx 10^{-7}$  in TW Hya (Hogerheijde et al. 2011). Evidently, gas-phase CO and  $\mathrm{H_2O}$  do not account for the majority of oxygen in TW Hya. Could oxygen be hiding in gas-phase  $\mathrm{O_2}$ ?

#### 2. OBSERVATIONS

Observations of the  $^{16}\mathrm{O}^{18}\mathrm{O}$   $N_J=2_1-0_1$  line at 233.946 GHz toward TW Hya were carried out as part of ALMA program 2019.1.01177.S (PI: Eistrup). Observations occurred on two nights in 2021, April 4 and April 6, for a combined time of 91 minutes on source. On April 4, there were 44 antennas and baselines of 15-1398 meters, and on April 6, 45 antennas and baselines of 15-1263 meters. J1058+0133 was adopted as the amplitude and bandpass calibrator, while J1037-2934 was used for phase calibration. The data were calibrated using the standard ALMA pipeline.

We searched for <sup>16</sup>O<sup>18</sup>O emission in both the image plane and the visibility plane, as described in more detail in the following section. Subsequent imaging and analysis were carried out using the Common Astronomy Software Applications (CASA) version 6.4 (McMullin et al. 2007). Continuum emission was subtracted using the task uvcontsub, applying a fit order of 1 and excluding edge channels. The data were imaged using tclean, initially with a natural weighting scheme to improve line sensitivity. The resulting beam is 0.59'' by 0.50'' with a position angle of  $-88^{\circ}$ , equivalent to a spatial resolution of 30 to 35 au at a distance of 60.1 pc (Bailer-Jones et al. 2018). The rms noise is 2.59 mJy beam<sup>-1</sup> for a channel width of 0.235 km s<sup>-1</sup>. For the matched filtering analysis, Earth's rotation was first corrected for using the CASA task cvel.

### 3. METHODS

We first created a Keplerian mask (Teague 2020) to use with the CASA *tclean* task. Due to the rotation of disks, we observe some emission to be shifted to higher or lower frequencies, so certain regions of the disk will be brighter in different channels. A Keplerian mask traces this emission pattern, based on the parameters of the disk, to improve the signal to noise of the integrated intensity (e.g. Salinas et al. 2017; Teague et al. 2022). We

assumed a systemic velocity of 2.86 km s<sup>-1</sup> (Favre et al. 2013), distance of 60.1 pc (Bailer-Jones et al. 2018), inclination =  $5.8^{\circ}$ , position angle =  $151^{\circ}$ , and stellar mass =  $0.81 \text{ M}_{\odot}$  (Teague et al. 2019). The mask was created using CO J = 3 - 2 emission data for TW Hya from Huang et al. (2018), and parameters optimized to fully trace the CO emission. Specifically, we set the target\_res = 0.4, which convolves the mask with a circular beam of 0.4 arcsec FWHM, and  $dV\theta = 500 \text{ m s}^{-1}$ , which affects the radially varying line width of emission. Two masks were then created for the  $O_2$  data, one with a radius set to 100 au (convolved to 120 au), and a second with a radius set to 240 au (convolved to 260 au, covering the extent of the CO emission). Both masks were used separately in cleaning, using a  $5\sigma$  threshold. The resulting image was the same in both cases because there were no values above  $5\sigma$  within either mask.

The tclean task has several parameters that can be varied to bring out faint emission. For example, the choice of weighting scheme and uvtaper can be tuned to give a higher weighting to shorter baselines to increase sensitivity, at the expense of a lower resolution. Because we were mainly interested in looking at the disk integrated flux, we did not need the full spatial resolution of the observations. We imaged the data with several combinations of the Briggs weighting robust parameter (Briggs 1995) and uvtaper. We used channel averaging as another method of revealing faint emission. The original channel width of the data was 0.078 km s<sup>-1</sup>, and we experimented with averaging 2, 3, and 5 channels together.

Matched filtering is a technique to detect weak emission in observational data (Loomis et al. 2018a). Matched filtering is applied in the visibility plane and therefore does not involve any imaging. It requires a filter that models the expected pattern of emission across velocity channels. The filter is Fourier transformed to generate a kernel that is then cross-correlated with the data. The result is an impulse response spectrum, with peaks indicating possible emission. For matched filtering, we used both Keplerian masks as filters (one with a 120 au radius, and one with a 260 au radius). It is possible that  $O_2$  emission covers a smaller area than these radii and could be hidden in the noise. However, Keplerian masks cover less area in edge channels, so a smaller mask is below the resolution of the images.

## 4. RESULTS

### 4.1. Imaging Results

Figure 1 shows the data imaged with natural weighting and velocity averaging to a channel size of  $0.235~\rm km~s^{-1}$ . For all attempted combinations of imaging param-

eters, no significant detection was found within either choice of mask. A spectrum, calculated within 260 au, is shown in Figure 2. The average rms noise level per channel in Figure 1 is 2.59 mJy beam<sup>-1</sup>. We calculated a disk integrated flux (for a velocity range of 4.69 km s<sup>-1</sup>) of  $-11.8 \pm 14.2$  mJy km s<sup>-1</sup> within 120 au, and  $7.4 \pm 18.0$  mJy km s<sup>-1</sup> within 260 au; i.e., at the noise level of the data, we do not detect <sup>16</sup>O<sup>18</sup>O  $N_J = 2_1 - 0_1$  emission.

### 4.2. Matched Filter Results

While we cannot see emission in the image plane, if there is emission just below the noise level, matched filtering has previously been successful at finding the signatures of line emission in other sources (Loomis et al. 2020), including when using a Keplerian mask as a template (Loomis et al. 2018a). By applying the Keplerian mask as our template, we provide an expectation for where rotating gas emission should appear spatially in our data. Since we do not know the extent of the  $O_2$ , we try both the 120 au and 260 au masks as templates. The results of matched filtering the data with these templates are presented in Figure 3. A  $3\sigma$  response at 0 km s<sup>-1</sup> would indicate emission from <sup>16</sup>O<sup>18</sup>O. Neither filter resulted in a  $3\sigma$  impulse response. We can conclusively say that the <sup>16</sup>O<sup>18</sup>O 233.946 GHz line is not detected at the sensitivity of the present measurements.

### 4.3. $O_2$ Upper Limits

How much oxygen could be hiding within our upper limit on  $^{16}\mathrm{O}^{18}\mathrm{O}$  emission? To estimate the total number of  $\mathrm{O}_2$  atoms from a single line, we explore a range of temperatures and assume its emission is in local thermodynamic equilibrium (LTE). Using the image-plane disk integrated flux limits from Section 4.1, we calculate the  $1\sigma$  upper limit on the maximum number of  $\mathrm{O}_2$  molecules that could be present in TW Hya, using the following adapted from Bergin et al. (2013).

$$F_l = \frac{\mathcal{N}_{^{16}O^{18}O} A_{20} h \nu f_u}{4\pi D^2} \tag{1}$$

 $F_l$  is the  $1\sigma$  flux calculated from our images,  $\mathcal{N}_{^{16}O^{18}O}$  is the number of  $^{16}O^{18}O$  molecules,  $A_{20}=1.33\times 10^{-8}~\mathrm{s}^{-1}$  is the Einstein A coefficient of the  $N_J=2_1-0_1$  transition (Marechal et al. 1997),  $\nu=233.94618$  GHz is the frequency of the  $N_J=2_1-0_1$  transition, and D=60.1 pc is the distance to TW Hya (Bailer-Jones et al. 2018). The fraction of molecules in the upper state is given by  $f_u=3.0\exp(-11.23~\mathrm{K}/T)/Q(T)$ , where 3 is the upper state degeneracy, 11.23 K is the upper state energy (Marechal et al. 1997),  $T_{\rm gas}$  is the gas temperature, and Q(T) is the partition function from the JPL spectral line catalog (Pickett et al. 1998; Mizushima & Yamamoto

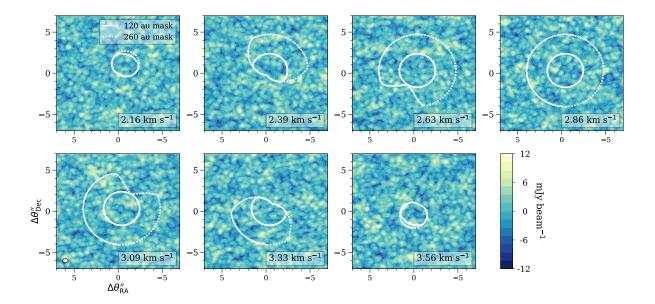
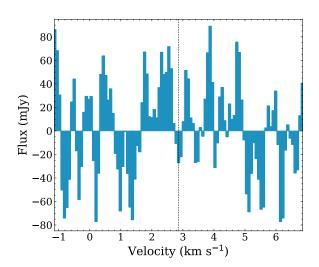


Figure 1. Channel maps of the intensity, centered on 233.946 GHz. The systemic velocity is  $2.86 \text{ km s}^{-1}$ . The two Keplerian masks are shown in white contours, and velocities are shown in the lower right of each panel. The beam size is  $0.59'' \times 0.50''$  and is shown in the lower left panel.



**Figure 2.** Spectrum of the  $O_2$  data for TW Hya, calculated within a 260 au region. The dashed line is the systemic velocity of 2.86 km s<sup>-1</sup>, centered on 233.946 GHz.

1991; Crownover et al. 1990; Steinbach & Gordy 1975; Amano & Hirota 1974). These partition functions are given for temperatures ranging from 9.4 K to 300.0 K, so this is the temperature range we use in our calculations. To get an upper limit on the total number of  $^{16}{\rm O}^{16}{\rm O}$  molecules, we assumed a  $^{16}{\rm O}^{16}{\rm O}/^{16}{\rm O}^{18}{\rm O}$  ratio of 280

(Taquet et al. 2018; Wilson & Rood 1994). We obtained an upper limit of  $(1.1-10.4)\times10^{49}$  O<sub>2</sub> molecules within 120 au, and  $(1.4-13.2)\times10^{49}$  molecules within 260 au, for a temperature range of 9.4 K to 300.0 K.

To give our result context, we also estimate the diskaveraged abundance of O<sub>2</sub> relative to hydrogen. To estimate the total hydrogen mass in the disk, we adopt the disk mass reported in Calahan et al. (2021), but we note that there are a wide range of mass values for the TW Hya disk in the literature (see Miotello et al. 2022). We adopt the Calahan et al. (2021) value of  $2.5 \times 10^{-2}$  M<sub> $\odot$ </sub> since it uses the HD line and multiple CO isotopologues to constrain the temperature structure. Assuming a molecular mass per hydrogen molecule of 2.8 (Kauffmann et al. 2008), this equates to  $2.1 \times 10^{55}$  hydrogen atoms in the whole disk. Within 120 au, we use the surface density profile from Calahan et al. (2021) to calculate a disk mass of  $1.8 \times 10^{-2} M_{\odot}$ , which equates to  $1.5 \times 10^{55}$  hydrogen atoms. Using these values, we estimate an  $O_2/H$  abundance of  $(7.2-70)\times 10^{-7}$  within 120 au, and  $(6.4-62) \times 10^{-7}$  within 260 au, for temperatures ranging from 9.4 K to 300.0 K. We will return to the implications of these results in Section 5.

### 4.4. Constraints from Serendipitous Molecular Lines

The SO  $N_J = 5_6 - 4_5$  and SO<sub>2</sub>  $N_J = 4_{(2,2)} - 3_{(1,3)}$  lines at 219.949 GHz and 235.152 GHz, respectively, were also included in the observational set-up. Given that

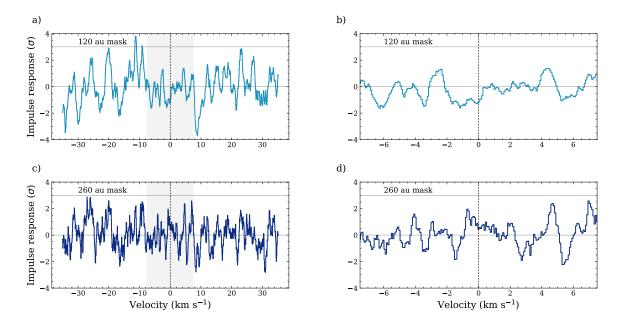


Figure 3. Matched filtering response for the  $^{16}\mathrm{O}^{18}\mathrm{O}$  data, with impulse response on the y-axis and velocity on the x-axis. The 233.946 GHz transition is centered at 0 km s<sup>-1</sup> and is denoted by the vertical dashed line. The two horizontal lines are at  $0\sigma$  and  $3\sigma$ . The gray region in the left plots is the range of velocities covered in the right plots. a) 120 au filter, covering all channels. b) zoom-in of the shaded region in panel a. c) 260 au filter, covering all channels. d) zoom-in of the shaded region in panel c.

these molecules might be prominent oxygen carriers, we searched for emission from these lines using similar techniques as for <sup>16</sup>O<sup>18</sup>O. Neither line was detected above  $3\sigma$  with imaging or matched filtering (see Appendix A). The disk integrated flux for the SO line is  $-0.05 \pm 12.5$ mJy km s $^{-1}$  within 120 au and  $-21.4 \pm 21.2$  mJy km  $s^{-1}$  within 260 au (covering a range of 4.99 km  $s^{-1}$ ). For SO<sub>2</sub>, the flux is  $24.4 \pm 14.8$  mJy km s<sup>-1</sup> within 120 au and  $34.3 \pm 24.5 \text{ mJy km s}^{-1}$  within 260 au (covering a range of  $4.67 \text{ km s}^{-1}$ ). We modified Equation 1 for SO and SO<sub>2</sub>, using values from LAMDA (Schöier et al. 2005) and CDMS (Müller et al. 2001), and partition functions from the JPL spectral line catalog (Pickett et al. 1998; Amano & Hirota 1974; Clark & De Lucia 1976; Helminger & De Lucia 1985; Lovas 1985; Alekseev et al. 1996). We calculate a  $1\sigma$  upper limit of SO/H =  $(2.4-10)\times 10^{-13}$  within 120 au and  $(2.9-12)\times 10^{-13}$ within 260 au, and  $SO_2/H = (7.9 - 197) \times 10^{-13}$  within 120 au and  $(9.1 - 229) \times 10^{-13}$  within 260 au, for a temperature range of 9.4 K to 300.0 K.

We also report a serendipitous detection of the C<sup>15</sup>N  $N_J = 2_{5/2} - 1_{3/2}$  hyperfine transitions, F = 2 - 1 and F = 3 - 2, at 219.93404 GHz and 219.93482 GHz, respectively. Using matched filtering with the 120 au Keplerian mask, we obtained a  $7\sigma$  filter response. The emission is visible in images (not shown), with an integrated flux of 113.5±17.0 mJy km s<sup>-1</sup> for a range of 2.33

km s<sup>-1</sup>, calculated within a 200 au circular region covering visible emission. For these images, we used Briggs weighting (robust = 2) and a uvtaper of 0.3 arcsec. The flux per channel is shown in Figure 4. C<sup>15</sup>N has previously been detected in TW Hya through its N=3-2 transition (Hily-Blant et al. 2017). They used two methods to calculate an integrated flux of 150  $\pm$  20 mJy km s<sup>-1</sup> and 160  $\pm$  13 mJy km s<sup>-1</sup>, the first of which is consistent with our value.

## 5. DISCUSSION

How does  $O_2$  stack up compared to other known oxygen carriers? Figure 5 shows our upper limits on  $O_2$  abundance as a function of temperature, compared to the solar oxygen abundance and known abundances of other major oxygen-carrying species in the ISM and in TW Hya. Since CO and  $H_2O$  each contain one oxygen atom, their abundances relative to hydrogen can be directly compared to the solar oxygen abundance (e.g., if all oxygen were in CO, then the CO/H abundance would equal the O/H value).  $O_2$ , on the other hand, contains two oxygen atoms, so should be multiplied by two to compare with the solar oxygen abundance.

In TW Hya, both CO gas and  $H_2O$  gas are several orders of magnitude below solar oxygen abundance; neither molecule is a major reservoir of oxygen. Our upper limit shows that gas-phase  $O_2$  is also not a major carrier

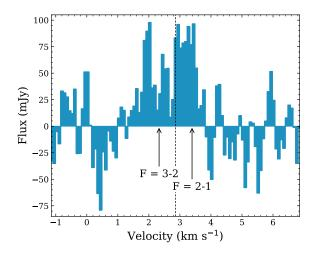


**Figure 4.** Spectrum of the C<sup>15</sup>N detection in TW Hya, calculated within a 200 au circular region. The two transitions are N=2-1, J=5/2-3/2 transitions, F=3-2 and F=2-1. The systemic velocity of 2.86 km s<sup>-1</sup>, centered on the average of the two emission frequencies, is marked with the dashed line.

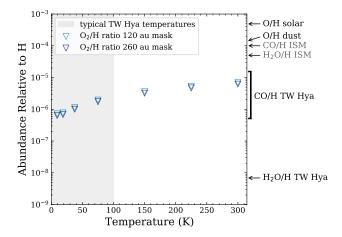


**Figure 5.** Upper limits on  $O_2$  in TW Hya as a function of temperature. The shaded region shows typical temperatures in TW Hya (see Bergin & Cleeves 2018), the light blue and dark blue open triangles show the upper limits on  $O_2$  abundance within 120 au and 260 au, respectively. Values for solar oxygen abundance (Asplund et al. 2009) and other known oxygen-carrying species are shown along the right axis. For dust, we assumed a value of  $1.4 \times 10^{-4}$  from Whittet (2010). From top to bottom, the remaining values used are from Ripple et al. (2013); van Dishoeck et al. (2013); Favre et al. (2013); Zhang et al. (2013).

of oxygen. Other oxygen-carrying molecules that have been detected in TW Hya include HCO<sup>+</sup> (van Dishoeck et al. 2003), H<sub>2</sub>CO (Öberg et al. 2017), CH<sub>3</sub>OH (Walsh et al. 2016), and HCOOH (Favre et al. 2018), but these molecules were all detected at too low an abundance to complete the oxygen budget relative to solar values. The majority of oxygen in TW Hya has not been detected, leading to several possibilities, which we discuss further.

Our upper limits on gas-phase  $O_2$  are not constraining enough to rule out protoplanetary disks as the origin of  $O_2$  in comets, as water vapor in TW Hya is detected in low abundance (Zhang et al. 2013). Comets 67P and 1P/Halley were observed to have high  $O_2/H_2O$  ratios of about 0.04 (Bieler et al. 2015; Rubin et al. 2015), whereas our upper limits on gas-phase  $O_2$  are about two orders of magnitude more abundant than detected water vapor in TW Hya (see Figure 5).

One possibility for the low detections of gas-phase oxygen carriers is that oxygen is frozen out, so it cannot be detected easily. Due to the low temperatures of disks, we expect many molecules (like H<sub>2</sub>O) to exist mostly in the ice-phase, but several processes can return molecules to the gas-phase throughout the entire disk. Photodesorption occurs when ultraviolet photons strike a molecule on the surface of a grain, causing the molecule to break off from the grain. It depends on the photon flux, as well as the binding energy of the molecule. Öberg et al. (2009) studied the photodesorption yield of H<sub>2</sub>O and found that the main products are H<sub>2</sub>O and OH. They also found that at high temperatures (100 K), up to 20% of the ice desorbs as  $O_2$ . Du et al. (2017) searched for cold water vapor in 13 protoplanetary disks, only detecting it in low abundance in two disks, and in the stacked spectrum of four other disks. They model the disk chemistry and find that, to match observations, the abundance of gas-phase oxygen must be reduced by a factor of 100 or more. They propose that oxygen (in the form of H<sub>2</sub>O and CO) freezes onto dust grains, which then settles to the midplane (Hogerheijde et al. 2011; Bergin et al. 2016). This process primarily occurs in the outer disk; in the inner disk (within 15 au), temperatures are higher and frozen molecules may return to the gas phase. Grain size may also play a role in molecular abundances. Eistrup et al. (2022) modeled disk chemistry, taking into account grain size. They found that larger grain sizes result in a lower gas-phase O<sub>2</sub> abundance and a higher H<sub>2</sub>O ice abundance, relative to the abundances produced using a fiducial  $0.1\mu m$  grain size. As grain size increases, the surface area decreases, which decreases the number of grain surface-reactions and gasgrain interactions that can occur.

Another possibility is that there is a large amount of oxygen in gas-phase molecules that we have not yet observed. Overall, the most abundant molecules detected in comets are H<sub>2</sub>O, CO<sub>2</sub>, and CO (Rubin et al. 2020). As discussed already, H<sub>2</sub>O and CO have been detected in disks in low abundance. Models by Eistrup et al. (2018) predict  $CO_2/H$  abundances of up to  $\approx 10^{-4}$  in disks.  $CO_2$  gas is difficult to observe in disks because, like  $O_2$ , it is symmetric and lacks a permanent dipole moment. CO<sub>2</sub> has been detected in the disk within 3 au of AA Tauri (Carr & Najita 2008), using Spitzer Space Telescope observations in the mid-infrared. JWST, however, can detect ice absorption features in the infrared, including CO<sub>2</sub> and H<sub>2</sub>O ices, and is already providing insight into oxygen-carrying molecules in disks (e.g. Yang et al. 2022; Grant et al. 2023; McClure et al. 2023).

### 6. CONCLUSIONS

We searched for but did not detect emission from gasphase  $^{16}\mathrm{O}^{18}\mathrm{O}$  in the protoplanetary disk around TW Hya. We used various imaging techniques along with matched filtering, and used our results to determine an upper limit on gas-phase  $\mathrm{O}_2$  in TW Hya.

- The isotopologue  $^{16}O^{18}O$  was not detected in TW Hya, leading to an upper limit on the abundance of  $O_2$  of  $(7.2-70)\times 10^{-7}$  relative to H if the emission is contained within 120 au. For the whole disk, the upper limit is  $(6.4-62)\times 10^{-7}$ . This limit is 2-3 orders of magnitude lower than the solar oxygen abundance, so gas-phase  $O_2$  is not a major reservoir for oxygen in TW Hya. Taking into account other existing molecular detections in TW Hya, the main oxygen-carrier(s) remain undetected.
- We place sensitive upper limits on the SO and SO<sub>2</sub> lines at 219.949 GHz and 235.152 GHz, respectively. We calculated an upper limit of SO/H =  $(2.4-10)\times 10^{-13}$  within 120 au and  $(2.9-12)\times 10^{-13}$  within 260 au, and of SO<sub>2</sub>/H =  $(7.9-197)\times 10^{-13}$  within 120 au and  $(9.1-229)\times 10^{-13}$  within 260 au. These results suggest oxygen is not bound up with sulfur either.
- We detect the isotopologue  $C^{15}N$  at the  $7\sigma$  level using matched filtering, and calculate an integrated flux of  $113.5 \pm 17.0$  mJy km s<sup>-1</sup>.

It is difficult to determine the main reservoir of oxygen in disks because of the many solid and gaseous forms oxygen may take (e.g. frozen  $\rm H_2O$ ,  $\rm CO$ ,  $\rm CO_2$ ; gas-phase  $\rm O_2$ ,  $\rm CO_2$ ). More observations of disks are necessary to search for this missing reservoir. Focusing on TW Hya, future searches for other gas-phase molecules, such as isotopologues of  $\rm CO_2$ , would provide more insight on oxygen. Alternatively, searches for gas-phase  $\rm ^{16}O^{18}O$  in other disks, could prove interesting. Observations of ices, especially with JWST, will also be helpful.

#### ACKNOWLEDGMENTS

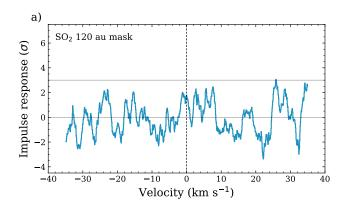
B.J.W. acknowledges support from the Virginia Initiative on Cosmic Origins (VICO). L.I.C. acknowledges support from the David and Lucile Packard Foundation, Research Corporation for Science Advancement Cottrell Fellowship, NASA ATP 80NSSC20K0529, NSF grant no. AST-2205698, and SOFIA Award 09-0183. C.E. acknowledges support from VICO. J.P.R. acknowledges support from the NASA Astrophysics Theory Program under grant no. 80NSSC20K0533, from the National Science Foundation (NSF) under grant nos. AST-1910106 and AST-1910675, and from the Virginia Initiative on Cosmic Origins. This paper makes use of the following ALMA data: ADS/JAO.ALMA#2019.1.01177.S. ALMA is a partnership of ESO (representing its member states), NSF (USA) and NINS (Japan), together with NRC (Canada) and NSC and ASIAA (Taiwan), in cooperation with the Republic of Chile. The Joint ALMA Observatory is operated by ESO, AUI/NRAO and NAOJ.

Facilities: ALMA

Software: Astropy (Astropy Collaboration et al. 2013), CASA (McMullin et al. 2007), Keplerian Mask (Teague 2020), VISIBLE (Loomis et al. 2018b)

#### A. MATCHED FILTER RESULTS: OTHER TRANSITIONS

The matched filtering response for the data containing the  $SO_2$  and SO transitions is shown in Figure 6. In both cases, the 120 au filter was used, and neither  $SO_2$  nor SO were detected at the  $3\sigma$  level or above. The  $7\sigma$  peak at about 20 km s<sup>-1</sup> in the SO spectrum is the  $C^{15}N$  detection.



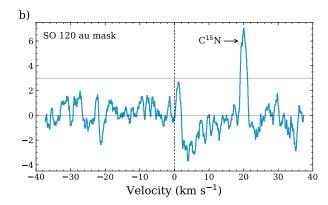


Figure 6. Matched filtering response for the data containing the  $SO_2$  and SO transitions, with impulse response on the y-axis and velocity on the x-axis. The two horizontal lines are at  $0\sigma$  and  $3\sigma$ . a)  $SO_2$  transition, centered at 235.152 GHz b)  $SO_3$  transition, centered at 219.949 GHz. The  $7\sigma$  peak is the  $C_3$  detection.

#### REFERENCES

Alekseev, E. A., Dyubko, S. F., Ilyushin, V. V., & Podnos, S. V. 1996, Journal of Molecular Spectroscopy, 176, 316, doi: 10.1006/jmsp.1996.0092

Amano, T., & Hirota, E. 1974, Journal of Molecular Spectroscopy, 53, 346,

doi: 10.1016/0022-2852(74)90071-X

Ansdell, M., Williams, J. P., van der Marel, N., et al. 2016, ApJ, 828, 46, doi: 10.3847/0004-637X/828/1/46

Asplund, M., Amarsi, A. M., & Grevesse, N. 2021, A&A, 653, A141, doi: 10.1051/0004-6361/202140445

Asplund, M., Grevesse, N., Sauval, A. J., & Scott, P. 2009, ARA&A, 47, 481,

doi: 10.1146/annurev.astro.46.060407.145222

Astropy Collaboration, Robitaille, T. P., Tollerud, E. J., et al. 2013, A&A, 558, A33,

doi: 10.1051/0004-6361/201322068

Bailer-Jones, C. A. L., Rybizki, J., Fouesneau, M., Mantelet, G., & Andrae, R. 2018, AJ, 156, 58, doi: 10.3847/1538-3881/aacb21

Balsiger, H., Altwegg, K., Bochsler, P., et al. 2007, SSRv, 128, 745, doi: 10.1007/s11214-006-8335-3

Bergin, E. A., & Cleeves, L. I. 2018, in Handbook of Exoplanets, ed. H. J. Deeg & J. A. Belmonte, 137, doi: 10.1007/978-3-319-55333-7\_137 Bergin, E. A., Du, F., Cleeves, L. I., et al. 2016, ApJ, 831, 101, doi: 10.3847/0004-637X/831/1/101

Bergin, E. A., Cleeves, L. I., Gorti, U., et al. 2013, Nature, 493, 644, doi: 10.1038/nature11805

Bieler, A., Altwegg, K., Balsiger, H., et al. 2015, Nature, 526, 678, doi: 10.1038/nature15707

Briggs, D. S. 1995, in American Astronomical SocietyMeeting Abstracts, Vol. 187, American AstronomicalSociety Meeting Abstracts, 112.02

Calahan, J. K., Bergin, E., Zhang, K., et al. 2021, ApJ, 908, 8, doi: 10.3847/1538-4357/abd255

Carr, J. S., & Najita, J. R. 2008, Science, 319, 1504, doi: 10.1126/science.1153807

Clark, W. W., & De Lucia, F. C. 1976, Journal of Molecular Spectroscopy, 60, 332, doi: 10.1016/0022-2852(76)90136-3

Cleeves, L. I., Bergin, E. A., Qi, C., Adams, F. C., & Öberg, K. I. 2015, ApJ, 799, 204, doi: 10.1088/0004-637X/799/2/204

Crownover, R. L., De Lucia, F. C., & Herbst, E. 1990, ApJL, 349, L29, doi: 10.1086/185643

Du, F., Bergin, E. A., Hogerheijde, M., et al. 2017, ApJ, 842, 98, doi: 10.3847/1538-4357/aa70ee

Dutrey, A., Guilloteau, S., & Simon, M. 1994, A&A, 286, 149

- Eistrup, C., Cleeves, L. I., & Krijt, S. 2022, A&A, 667, A121, doi: 10.1051/0004-6361/202243981
- Eistrup, C., Walsh, C., & van Dishoeck, E. F. 2018, A&A, 613, A14, doi: 10.1051/0004-6361/201731302
- Favre, C., Cleeves, L. I., Bergin, E. A., Qi, C., & Blake, G. A. 2013, ApJL, 776, L38, doi: 10.1088/2041-8205/776/2/L38
- Favre, C., Fedele, D., Semenov, D., et al. 2018, ApJL, 862, L2, doi: 10.3847/2041-8213/aad046
- Goldsmith, P. F., Liseau, R., Bell, T. A., et al. 2011, ApJ, 737, 96, doi: 10.1088/0004-637X/737/2/96
- Grant, S. L., van Dishoeck, E. F., Tabone, B., et al. 2023, ApJL, 947, L6, doi: 10.3847/2041-8213/acc44b
- Helminger, P. A., & De Lucia, F. C. 1985, Journal of Molecular Spectroscopy, 111, 66, doi: 10.1016/0022-2852(85)90069-4
- Hily-Blant, P., Magalhaes, V., Kastner, J., et al. 2017, A&A, 603, L6, doi: 10.1051/0004-6361/201730524
- Hogerheijde, M. R., Bergin, E. A., Brinch, C., et al. 2011, Science, 334, 338, doi: 10.1126/science.1208931
- Huang, J., Andrews, S. M., Cleeves, L. I., et al. 2018, ApJ, 852, 122, doi: 10.3847/1538-4357/aaa1e7
- Kauffmann, J., Bertoldi, F., Bourke, T. L., Evans, N. J., I., & Lee, C. W. 2008, A&A, 487, 993, doi: 10.1051/0004-6361:200809481
- Liseau, R., Goldsmith, P. F., Larsson, B., et al. 2012, A&A, 541, A73, doi: 10.1051/0004-6361/201118575
- Long, F., Herczeg, G. J., Pascucci, I., et al. 2017, ApJ, 844, 99, doi: 10.3847/1538-4357/aa78fc
- Loomis, R. A., Öberg, K. I., Andrews, S. M., et al. 2018a, AJ, 155, 182, doi: 10.3847/1538-3881/aab604
- Loomis, R. A., Oberg, K. I., Andrews, S. M., et al. 2018b, VISIBLE: VISIbility Based Line Extraction, Astrophysics Source Code Library, record ascl:1802.006. http://ascl.net/1802.006
- Loomis, R. A., Öberg, K. I., Andrews, S. M., et al. 2020, ApJ, 893, 101, doi: 10.3847/1538-4357/ab7cc8
- Lovas, F. J. 1985, Journal of Physical and Chemical Reference Data, 14, 395, doi: 10.1063/1.555729
- Luspay-Kuti, A., Mousis, O., Lunine, J. I., et al. 2018, SSRv, 214, 115, doi: 10.1007/s11214-018-0541-2
- Luspay-Kuti, A., Mousis, O., Pauzat, F., et al. 2022, Nature Astronomy, 6, 724, doi: 10.1038/s41550-022-01614-1
- Marechal, P., Viala, Y. P., & Pagani, L. 1997, A&A, 328, 617
- McClure, M. K., Rocha, W. R. M., Pontoppidan, K. M., et al. 2023, Nature Astronomy, 7, 431, doi: 10.1038/s41550-022-01875-w
- McGuire, B. A. 2022, ApJS, 259, 30, doi: 10.3847/1538-4365/ac2a48

- McMullin, J. P., Waters, B., Schiebel, D., Young, W., & Golap, K. 2007, in Astronomical Society of the Pacific Conference Series, Vol. 376, Astronomical Data Analysis Software and Systems XVI, ed. R. A. Shaw, F. Hill, & D. J. Bell, 127
- Miotello, A., Kamp, I., Birnstiel, T., Cleeves, L. I., & Kataoka, A. 2022, arXiv e-prints, arXiv:2203.09818. https://arxiv.org/abs/2203.09818
- Mizushima, M., & Yamamoto, S. 1991, Journal of Molecular Spectroscopy, 148, 447, doi: 10.1016/0022-2852(91)90400-5
- Müller, H. S. P., Thorwirth, S., Roth, D. A., & Winnewisser, G. 2001, A&A, 370, L49, doi: 10.1051/0004-6361:20010367
- Öberg, K. I., Linnartz, H., Visser, R., & van Dishoeck,
  E. F. 2009, ApJ, 693, 1209,
  doi: 10.1088/0004-637X/693/2/1209
- Öberg, K. I., Guzmán, V. V., Merchantz, C. J., et al. 2017, ApJ, 839, 43, doi: 10.3847/1538-4357/aa689a
- Pickett, H. M., Poynter, R. L., Cohen, E. A., et al. 1998, JQSRT, 60, 883, doi: 10.1016/S0022-4073(98)00091-0
- Przybilla, N., Nieva, M.-F., & Butler, K. 2008, ApJL, 688, L103, doi: 10.1086/595618
- Ripple, F., Heyer, M. H., Gutermuth, R., Snell, R. L., & Brunt, C. M. 2013, MNRAS, 431, 1296, doi: 10.1093/mnras/stt247
- Rubin, M., Altwegg, K., van Dishoeck, E. F., & Schwehm, G. 2015, ApJL, 815, L11, doi: 10.1088/2041-8205/815/1/L11
- Rubin, M., Engrand, C., Snodgrass, C., et al. 2020, SSRv, 216, 102, doi: 10.1007/s11214-020-00718-2
- Salinas, V. N., Hogerheijde, M. R., Mathews, G. S., et al. 2017, A&A, 606, A125, doi: 10.1051/0004-6361/201731223
- Schöier, F. L., van der Tak, F. F. S., van Dishoeck, E. F., & Black, J. H. 2005, A&A, 432, 369, doi: 10.1051/0004-6361:20041729
- Steinbach, W., & Gordy, W. 1975, PhRvA, 11, 729, doi: 10.1103/PhysRevA.11.729
- Taquet, V., van Dishoeck, E. F., Swayne, M., et al. 2018, A&A, 618, A11, doi: 10.1051/0004-6361/201833175
- Teague, R. 2020, richteague/keplerian\_mask: Initial Release, 1.0, Zenodo, doi: 10.5281/zenodo.4321137
- Teague, R., Bae, J., Huang, J., & Bergin, E. A. 2019, ApJL, 884, L56, doi: 10.3847/2041-8213/ab4a83
- Teague, R., Bae, J., Andrews, S. M., et al. 2022, ApJ, 936, 163, doi: 10.3847/1538-4357/ac88ca
- van Dishoeck, E. F., Herbst, E., & Neufeld, D. A. 2013, Chemical Reviews, 113, 9043, doi: 10.1021/cr4003177

- van Dishoeck, E. F., Thi, W. F., & van Zadelhoff, G. J. 2003, A&A, 400, L1, doi: 10.1051/0004-6361:20030091
- van Dishoeck, E. F., Kristensen, L. E., Mottram, J. C., et al. 2021, A&A, 648, A24,
  - doi: 10.1051/0004-6361/202039084
- Walsh, C., Nomura, H., & van Dishoeck, E. 2015, A&A, 582, A88, doi: 10.1051/0004-6361/201526751
- Walsh, C., Loomis, R. A., Öberg, K. I., et al. 2016, ApJL, 823, L10, doi: 10.3847/2041-8205/823/1/L10
- Whittet, D. C. B. 2010, ApJ, 710, 1009, doi: 10.1088/0004-637X/710/2/1009
- Wilson, T. L., & Rood, R. 1994, ARA&A, 32, 191, doi: 10.1146/annurev.aa.32.090194.001203
- Yang, Y.-L., Green, J. D., Pontoppidan, K. M., et al. 2022, ApJL, 941, L13, doi: 10.3847/2041-8213/aca289
- Zhang, K., Pontoppidan, K. M., Salyk, C., & Blake, G. A. 2013, ApJ, 766, 82, doi: 10.1088/0004-637X/766/2/82